Mathematical appendix:

Oligomerization and feedback on membrane recruitment stabilize PAR-3 asymmetries in *C. elegans* zygotes

Charles F. Lang, Alexander Anneken, Ondrej Maxian, and Edwin M. Munro

This part of the supplemental material deals with our mathematical model of PAR-3 kinetics, which is based strongly on previous work by some of us [9]. In our model, we let $A_n(x)$ be the density (number/length) of membrane-bound oligomers of size n at point x. The density of each oligomer size evolves according to the equations [9, Eq. (1)]

$$\partial_t A_1 = D_A \partial_x^2 A_1 + \left(k_A^{\text{on}} + k_A^+ f_A^+(A)\right) A_{\text{cyto}} - k_A^{\text{off}} A_1 \tag{M1a}$$
$$+ 2k_A^{\text{dp}} A_2 - 2k_A^{\text{p}} A_1^2 + \sum_{n=3}^{N} \left(k_A^{\text{dp}} A_n - k_A^{\text{p}} A_1 A_{n-1}\right)$$
$$\partial_t A_n = k_A^{\text{p}} A_1 \left(A_{n-1} - A_n\right) - k_A^{\text{dp}} \left(A_n - A_{n+1}\right) \qquad N > n \geq 2 \tag{M1b}$$
$$\partial_t A_N = k_A^{\text{p}} A_1 A_{N-1} - k_A^{\text{dp}} A_N \tag{M1c}$$
$$A_{\text{cyto}} = \frac{1}{hL}\left(A^{(\text{Tot})} L - \int_0^L A(x)\, dx\right) \qquad A(x) = \sum_{n=1}^{N} n A_n(x). \tag{M1d}$$

A schematic diagram of this model can be found in Fig. 3A, and more details on its assumptions can be found in [9]. Table 1 lists the parameters we use here. Briefly, the first line of (M1a) describes the evolution of monomers, which bind directly from the cytoplasm and unbind from the membrane in monomer form. The second line of (M1a), combined with (M1b) and (M1c) represent polymerization dynamics on the membrane. There the depolymerization rate k_A^{dp} is the rate at which oligomers of size n become oligomers of size $n-1$. Because we assume oligomers are linear, this event can occur from either side, and as such the rate k_A^{dp} is twice that observed in single-molecule imaging. The cytoplasmic concentration is determined in (M1d) from the conservation of total protein in the system, where $A(x)$ is the total bound density at each point on the membrane.

The equations (M1) contain two important simplifying assumptions. First, our experimental data (Fig. 3K) shows that the unbinding kinetics of oligomers follows a power-law decay, with each additional monomer increasing the oligomer residence time by a factor of 4. Because of this, we neglect the unbinding of oligomers into the cytoplasm, as in [9]. Second, experiments have provided evidence for the direct positive feedback term $k_A^+ f_A^+(A)$. Previous simulations [9] have shown that direct binding and unbinding of cytoplasmic monomers to membrane-bound oligomers does not alter the qualitative behavior of the model (in terms of the types of steady states), but effectively weakens or strengthens the feedback strength depending on the regime considered. For this reason, we will not directly model the (un)binding of cytoplasmic monomers to membrane-bound oligomers, instead assuming that this is implicit in the feedback strength.

1 Nondimensionalization and parameter estimation

Because the total amount of PAR-3 in the system is unknown, and because each embryo has a slightly different length, it is necessary to scale the equations by appropriate time, length, and density scales. A sensible timescale for the system is the time a typical PAR-3 molecule spends on the membrane. Since polymerization dynamics are much slower than unbinding, this timescale is roughly $1/k_A^{\mathrm{dp}}$. We define the dimensionless (hatted) variables

$$x = \hat{x}L, \qquad t = \hat{t}/k_A^{\mathrm{dp}}, \qquad A = \hat{A}A^{(\mathrm{Tot})}.$$

Substituting into (M1) gives the rewritten dynamics [9, Eq. 14]

$$\begin{aligned}
\partial_{\hat{t}}\hat{A}_1 &= \hat{D}_A\partial_{\hat{x}}^2 A_1 + \hat{K}_A^{\mathrm{on}}\left(1+\hat{K}_A^{\mathrm{f}}\hat{F}_A^+(\hat{A})\right)\left(1-\int_0^1 \hat{A}(x)\,d\hat{x}\right) - \hat{K}_A^{\mathrm{off}}\hat{A}_1 \\
&\quad + 2\hat{A}_2 - 2\hat{K}_A^{\mathrm{p}}{\hat{A}_1}^2 + \sum_{n=3}^{N}\left(\hat{A}_n - \hat{K}_A^{\mathrm{p}}\hat{A}_1\hat{A}_{n-1}\right) && \text{(M2a)}\\
\partial_{\hat{t}}\hat{A}_n &= \hat{K}_A^{\mathrm{p}}\hat{A}_1(\hat{A}_{n-1}-\hat{A}_n) - (\hat{A}_n - \hat{A}_{n+1}) \qquad N > n \geq 2 && \text{(M2b)}\\
\partial_t A_N &= \hat{K}_A^{\mathrm{p}}\hat{A}_1\hat{A}_{N-1} - \hat{A}_N && \text{(M2c)}\\
\hat{D}_A &= \frac{D_A}{L^2 k_A^{\mathrm{dp}}}, \quad \hat{K}_A^{\mathrm{on}} = \frac{k_A^{\mathrm{on}}}{k_A^{\mathrm{dp}}h}, \quad \hat{K}_A^{\mathrm{f}} = \frac{k_A^+ A^{(\mathrm{Tot})}}{k_A^{\mathrm{on}}}, \quad \hat{K}_A^{\mathrm{off}} = \frac{k_A^{\mathrm{off}}}{k_A^{\mathrm{dp}}}, && \text{(M2d)}\\
\hat{K}_A^{\mathrm{p}} &= \frac{k_A^{\mathrm{p}}A^{(\mathrm{Tot})}}{k_A^{\mathrm{dp}}}, \quad \hat{F}_A^+(\hat{A}) = \frac{f_A^+(A)}{A^{(\mathrm{Tot})}}.
\end{aligned}$$

This study gives accurate measurements for three of the PAR-3-related parameters: the diffusion coefficient $D_A = 0.1\ \mu\mathrm{m}^2/\mathrm{s}$, the detachment rate $k_A^{\mathrm{off}} = 3/\mathrm{s}$, and the *single molecule* depolymerization rate 0.08/s, which means that $k_A^{\mathrm{dp}} = 0.16/\mathrm{s}$. For lengthscales, a typical *C. elegans* embryo

has a roughly ellipsoidal shape, with half-axis lengths $27 \times 15 \times 15$ μm. As such, our model will be a 27×15 ellipse, which has perimeter $L = 134.6$ μm [6]. In our one-dimensional model, the cytoplasm has a "thickness" which is just the area of the ellipse 1272 μm^2 divided by the perimeter L, which gives $h = 9.5$ μm.

The experimental measurements leave the parameters $\hat{K}_A^{\rm on}$, $\hat{K}_A^{\rm p}$, and $\hat{K}_A^{\rm f}$ unknown. The parameters related to feedback will be handled in subsequent sections. To fit the polymerization rate, we first solve (M2) at steady state to obtain an exponential distribution of oligomer sizes [4, 9]

$$\hat{A}_n = \hat{K}_A^{\rm p}\hat{A}_1\hat{A}_{n-1} := \alpha\hat{A}_{n-1} \quad n \geq 2. \tag{M3}$$

This defines $\alpha = \hat{K}_A^{\rm p}\hat{A}_1$ as the coefficient of the exponential distribution of oligomer sizes. It follows that the total number of monomers is given by

$$\hat{A} = \sum_{n=1}^{N} n\alpha^{n-1}\hat{A}_1 \xrightarrow{N\to\infty} \frac{\hat{A}_1}{(1-\alpha)^2}. \tag{M4}$$

This equation can then be solved for $\hat{A}_1$ to obtain [9, Eq. (12)]

$$\hat{A}_1 = \frac{1 + 2\hat{A}\hat{K}_A^{\rm p} - \sqrt{1 + 4\hat{K}_A^{\rm p}\hat{A}}}{2\hat{A}\left(\hat{K}_A^{\rm p}\right)^2}, \tag{M5}$$

which gives the number of bound monomers as a function of the total bound $\hat{A}$. Thus, α can be written as a function of $\hat{A}$ and $\hat{K}_A^{\rm p}$. For this purpose, we consider *spd-5* (RNAi) embryos, where the PAR-3 density is roughly uniform throughout the cortex. In these embryos (as with wild-type embryos), the level of protein in late maintenance phase is roughly half of the late-interphase levels. Thus, an upper bound on the bound density is $\hat{A} = 0.5$. Since the mean oligomer size is $\alpha \approx 0.7$, we obtain $\hat{K}_A^{\rm p} = 15$ as a reasonable parameter for the polymerization dynamics.

2 The form of the feedback strength and resulting steady states

We now turn to models of feedback, which is the main focus of this supplement. Our goal in particular is to analyze the *stability* behavior with different feedback models, and use the qualitative behavior of the system to settle on a preferred model. To do this, it will be vital to understand the behavior near steady state. In the absence of diffusion, invoking the steady state (M3) for polymerization dynamics reduces the monomer equation (M2a) to a balance of the binding flux

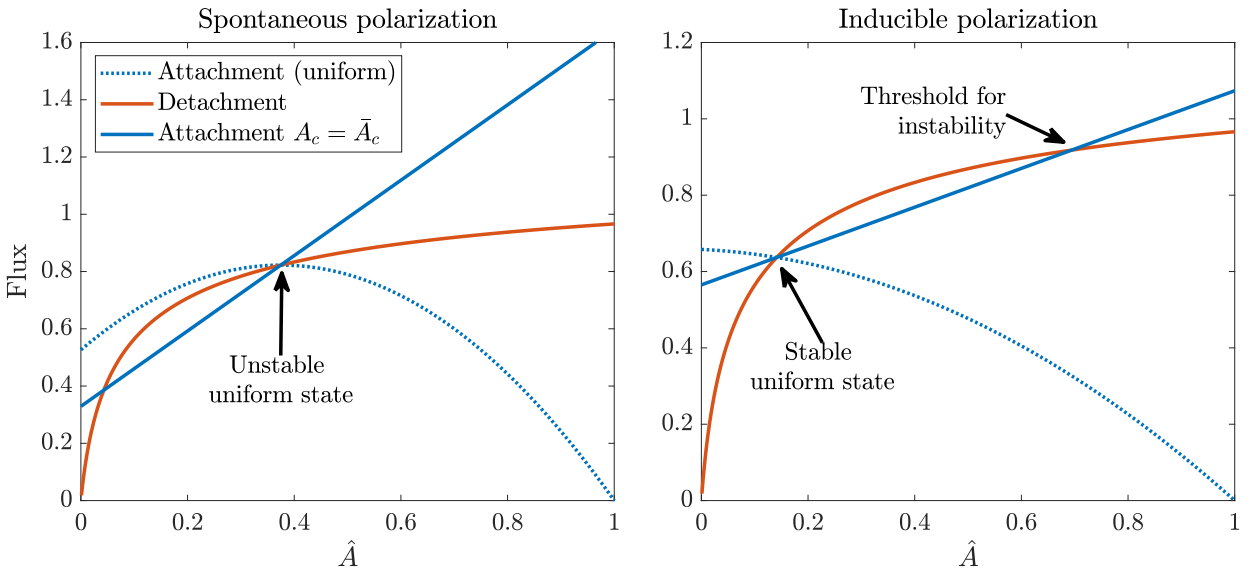

Figure M1: Flux plane analysis for linear feedback model (M7). The stability analysis is determined by how the attachment rate (solid blue line, with constant cytoplasmic concentration) compares to the detachment rate (red) near the steady state. In the left plot, the uniform state is unstable and spontaneous polarization is predicted, while in the right plot the uniform state is stable and polarization can be induced by large perturbations.

(which combines the basal binding rate and the feedback) and the unbinding flux,

$$0 = \underbrace{\hat{K}_A^{\text{on}}\left(1 + \hat{K}_A^{\text{f}}\hat{F}_A^{+}(\hat{A})\right)\hat{A}_c}_{\text{On flux}} - \underbrace{\hat{K}_A^{\text{off}}\hat{A}_1}_{\text{Off flux}} \tag{M6}$$

$$\hat{A}_c = \left(1 - \int_0^1 \hat{A}(x)\, d\hat{x}\right)$$

When the system is in a uniform state, the cytoplasmic concentration $\hat{A}_c = 1 - \hat{A}$, but this is not the case in polarized states. Thus when performing stability analysis, we need to consider *both* the case when $\hat{A}_c = 1 - \hat{A}$, and the case when it is constant and equal to its value at the uniform state.

2.1 Linear feedback model

Let us first consider the linear feedback model that was used previously in work by some of us [9]

$$f_A^{+}(A) = A \to \hat{F}_A^{+}(\hat{A}) = \hat{A}. \tag{M7}$$

As shown in Fig. M1, the behavior of this model falls into one of two cases:

1. The uniform state is unstable. This occurs when the feedback dominates the basal binding rate.

2. The uniform state is stable, but it is possible to induce polarization by driving the local concentration above some threshold.

According to our experimental observations in spd-5 (RNAi) embryos, the uniform state is in fact stable, which rules out scenario 1. Thus, we choose parameters that fall in the regime of scenario 2. Here we are strongly constrained by the fact that the anterior state (in wild-type) closely resembles the uniform state (*spd-5* (RNAi)), so the threshold for instability must lie close to the unstable uniform state. In Fig. M2(a), we show the flux plane for a set of parameters ($\hat{K}_A^{\mathrm{on}} = 0.8$ and $\hat{K}_A^{\mathrm{f}} = 1.4$) where this is the case.

The dynamics of the linearized feedback model are shown in Fig. M2(b). In the left panel, we see that perturbations to the uniform state are stable, which matches the observations in *spd-5* embryos. In the right panel, we see that polarized states are self-sustaining. The polarized state shown there initially shrinks down in both the "posterior" and "anterior" sides, reaching a quasi-stable state between $t = 5$ and $t = 20$ minutes. Then, as expected from our flux analysis, the anterior concentration grows and the posterior concentration shrinks, as there is nothing to stop the instability from growing. The timescale on which this occurs, however, is about 30 minutes (resulting from slow oligomerization dynamics), which is much longer than maintenance phase in live embryos.

Because of this important fact, it is impossible to say for certain that the linear feedback model is incorrect, though its tendency to focus the anterior cap is concerning. One hint we do get, however, is the key separation between the uniform state ($\hat{A} \approx 0.2$) and the enriched anterior state ($\hat{A} \approx 0.6$). This is a consequence of the model we have chosen; because the "anterior" state lies above a fixed point which is in turn above the uniform steady state, there has to be a good deal of space between the two points. This is *not* what we see in our embryos, where we observe a good match between the uniform state and anterior state.

2.2 Saturated feedback model with bistability

The data consequently argue for an alternative model: suppose that the uniform state was a stable state, but that for certain values of the feedback strength it could coexist with a depleted posterior state. In this case, rather than driving the anterior side above the uniform state, we would attain polarization by driving the posterior state down to a new stable state.

In order for this scenario to play out, the attachment flux at constant cytoplasmic concentration has to intersect the detachment curve three times (two stable fixed points and one unstable fixed

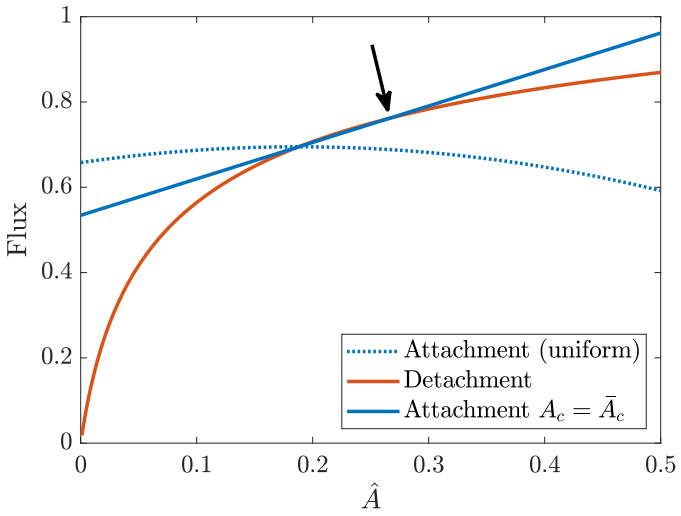

(a) Flux plane

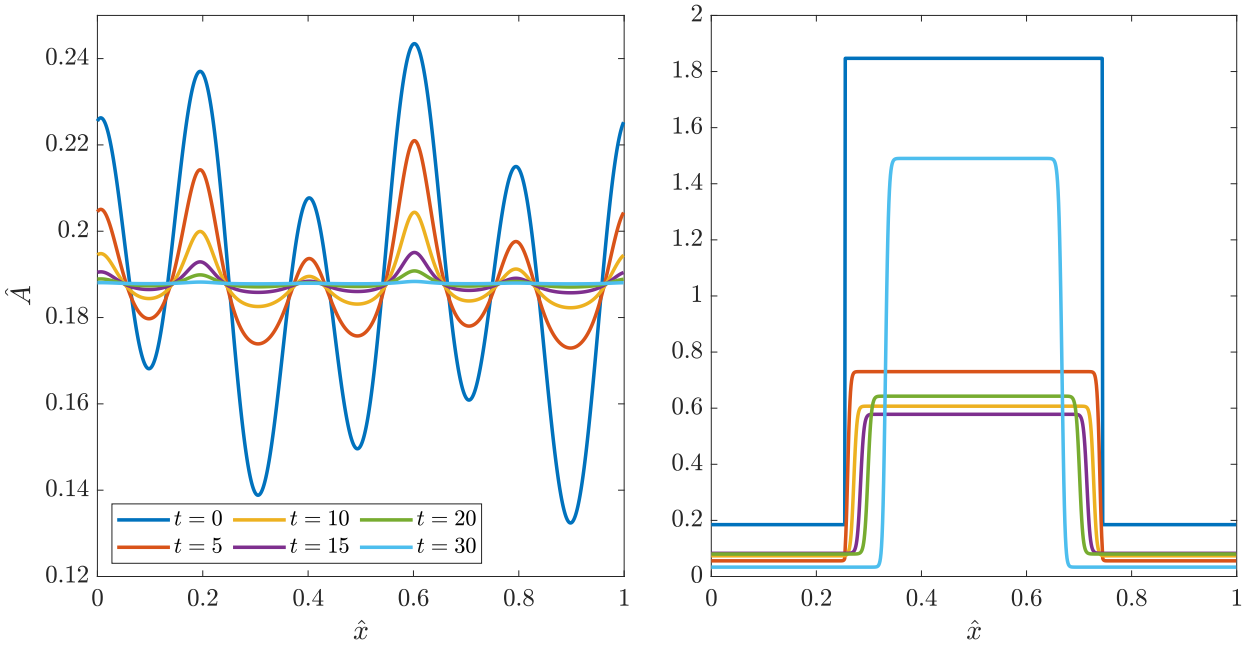

(b) Dynamics

Figure M2: Linear feedback model with our chosen parameters, $\hat{K}_A^{\text{on}} = 0.66$ and $\hat{K}_A^{\text{f}} = 1.6$. (a) Flux plane analysis. The uniform state is linearly stable, but perturbations *beyond the black arrow) can induce polarized states. (b) Dynamic trajectories starting from a perturbed uniform state (left), and a polarized state (right). Time is marked in minutes.

point in between), which is impossible with a linear feedback function. A simple way to accomplish this is by introducing saturation into the feedback curve,

$$f_A^+(A) = \min\left(A, A^{(\mathrm{Sat})}\right) \rightarrow \hat{F}_A^+(\hat{A}_1, \hat{A}_n) = \min\left(\hat{A}, \hat{A}^{(\mathrm{Sat})}\right). \tag{M8}$$

In order for the uniform state to be stable... Pick up here with the text.

A consequence of this is the introduction of a new parameter, $\hat{A}^{(\mathrm{Sat})}$, which expresses the PAR-3 saturation threshold. In wild-type embryos, it is possible to constrain this parameter from experimental observations. The stability of the uniform state implies that feedback has to saturate below the uniform state, so $\hat{A}^{(\mathrm{Sat})} < \hat{A}_u \approx 0.5$, which provides one constraint on the saturation. The second constraint comes from bistability; the system is only locally bistable at fixed cytoplasmic concentration when $\hat{A}^{(\mathrm{Sat})}$ is close to the uniform state (if $\hat{A}^{(\mathrm{Sat})}$ is too small the feedback becomes essentially constant and cannot generate bistability). Based on these considerations, we set $\hat{A}^{(\mathrm{Sat})} = 0.35$ in the wild-type system.

Once $\hat{A}^{(\mathrm{Sat})} = 0.35$ is set, there are two unknown parameters, the basal binding rate k_A^{on} and the strength of the feedback $\hat{K}_A^{\mathrm{f}}$. In Fig. M3, we set these two parameters based on three considerations

1. The uniform state is around $\hat{A}_u \approx 0.5$.
2. The polarized state has roughly a 10:1 ratio of A/P protein.
3. In the polarized state, $\hat{A} \approx 0.6$ on the anterior.

Figure M3 shows that the parameter choice $\hat{K}_A^{\mathrm{f}} = 2.8$ and $k_A^{\mathrm{on}} = 0.8$ μm/s approximately satisfies these three criteria. In dynamic simulations of the model (M2) with these parameters, dropping the local density of $\hat{A}$ below 85% of the uniform state gives rise to a polarized state, one example of which is shown in the right panel of Fig. M3. We have chosen parameters so that, in a situation where 50% of the domain is in the enriched state, there is about 10 times as much in the enriched state as the depleted state (see Fig. M4).

3 Systematic depletion of PAR-3 and how feedback changes

Thus far, we showed that experimental data are consistent with a model where the feedback (M8) has a "cap" at a point that sits just below the uniform steady state. But it is not clear how to scale the cap $\hat{A}^{(\mathrm{Sat})}$ when we move away from the wild-type parameters. To address this problem, we consider the PAR-3 depletion experiment in the final stages of the main text. We assume that

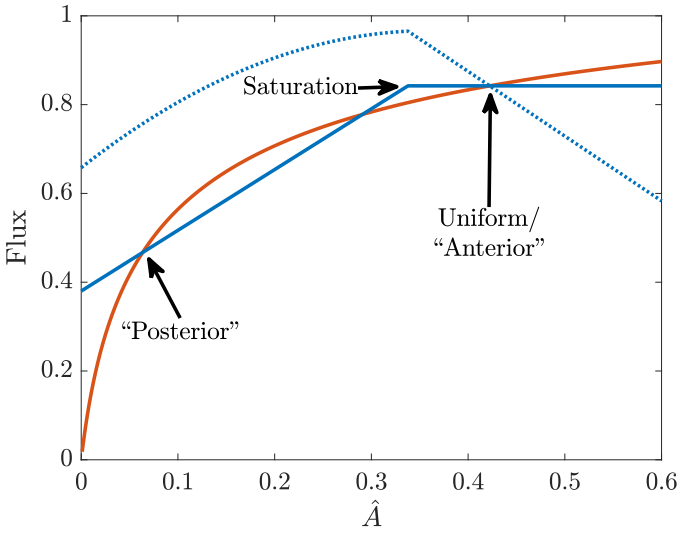

(a) Flux plane

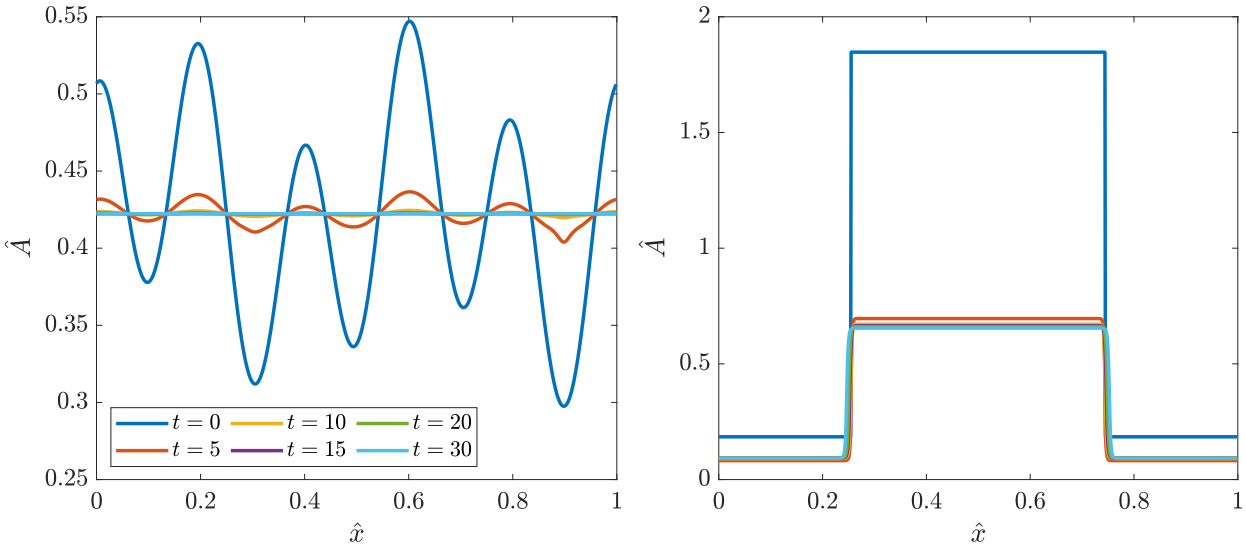

(b) Dynamics

Figure M3: Steady state analysis for capped linear feedback in the bistable case ($\hat{K}_A^{\text{on}} = 0.66$ and $\hat{K}_A^{\text{f}} = 3.6$). Left plot: The stability analysis is determined by how the attachment rate (solid blue line, with constant cytoplasmic concentration) compares to the detachment rate (red) near the steady state. The uniform state ($\hat{A}_u \approx 0.4$) is stable, and coexists with a depleted state. Right plot: the stable polarized state that results when we perturb away from the uniform state with these parameters.

Parameter	Description	Value	Units	Ref	Notes
L	Domain length	134.6	μm	[6]	radii 27×15 μm ellipse
h	Cytoplasmic "thickness"	9.5	μm	[6]	(area/circumference)
D_A	Monomeric PAR-3 diffusivity	0.1	$\mu\text{m}^2/\text{s}$		This study
k_A^{off}	Monomeric PAR-3 detachment rate	3	1/s		This study, Fig. 3K
k_A^{dp}	PAR-3 depolymerization rate	0.16	1/s		This study, Fig. 4E
$\hat{K}_A^{\text{p}}$	PAR-3 polymerization rate	15			Fit α in uniform state
$\hat{F}_A^+$	PAR-3 feedback function	$\min\left(\hat{A}, 0.35\right)$		[9]	Stable uniform state
N	Max oligomer size	50			Same results for larger N
$A^{(\text{Tot})}$	Maximum bound PAR-3 density	–	$\#/\mu$m		Contained in other unknowns

Table 1: Parameter values for the PAR-3 model (see (M2d) for the definitions of dimensionless parameters). Here we leave out parameters $\hat{K}_A^{\text{f}}$ and $\hat{K}_A^{\text{on}}$, which vary depending on the model being considered.

PAR-3 depletion removes some fraction of the total protein in the system, so that the total amount of protein is some fraction

$$F = A^{(\text{Tot})}/A_{\text{WT}}^{(\text{Tot})}.$$

of the wild type. The scalings in (M2d) clearly show how the dimensionless parameters $\hat{K}_A^{\text{p}}$ (polymerization) and $\hat{K}_A^{\text{f}}$ (feedback strength) should scale with F; thus, when doing simulations with $F \neq 1$ we set $\hat{K}_A^{\text{p}} = 20F$ and $\hat{K}_A^{\text{f}} = 2.8F$, so that polymerization and feedback get relatively weaker as we decrease the total amount of PAR-3.

The problem here is that we still do not know how to scale the feedback saturation threshold $\hat{A}^{(\text{Sat})}$ with F. We consider three hypotheses in this section:

1. The feedback saturates at a fixed *number* of monomers $A_0^{(\text{Sat})}$, which means that it gets harder to saturate as the amount of PAR-3 drops. In dimensionless variables, this corresponds to a saturation point $\hat{A}^{(\text{Sat})} = \hat{A}_{\text{WT}}^{(\text{Sat})}/F = 0.35/F$. For small F, this gives feedback which has *not* saturated at the uniform steady state (and in fact, as F decreases, in this model the feedback gets farther from saturation at the uniform steady state).

2. The feedback saturates at a fixed *percentage* of monomers $\hat{A}_0^{(\text{Sat})} = 0.35$ (constant in dimensionless variables, relatively decreasing in dimensional variables). This model is a slightly better-controlled version of the previous one; because the feedback always saturates at the same relative point, the anterior state cannot get too enriched. However, it still gives feedback which has not saturated at the uniform state when F is small.

By decoupling the saturation point from the uniform state, these first two models tend to give unstable uniform states and high A/P ratios for intermediate protein amounts. Thus, another option is to simply employ the same procedure for any choice of $\hat{K}_A^{\mathrm{f}}$ and $\hat{K}_A^{\mathrm{p}}$ that we did for the base wild-type parameters; that is, scale the saturation point so that the uniform state is always stable. This gives rise to a third option for the feedback

3. The feedback saturates at a fixed percentage ($\approx 90\%$, determined from the default parameters) of the uniform state. In this model, we solve for the uniform state $\hat{A}_u$ assuming the feedback is saturated at $0.93\hat{A}_u$, then substitute to obtain the saturation level in non-uniform states. Examples of this process are shown in Fig. **??**, where we see feedback saturating at a smaller percentage of bound PAR-3 when there is less of it.

In this option, the uniform state is always stable by design, with bistability coming when feedback is high enough to intersect the detachment curve three times. Choosing the saturation point at a fixed level of the uniform state gives precise control over the pitchfork bifurcation that results (Fig, **??**), with the uniform state always being stable and bistability occurring at 90% or higher PAR-3 amounts.

3.1 Replicating experimental conditions

To differentiate our feedback models, we compare their dynamics with the experimental results of a PAR-3 depletion experiment. To simulate experimental conditions, we first set the fraction F of total PAR-3, then scale the dimensionless feedback strength and polymerization rate accordingly. To mimic the end of establishment phase, we initialize a simulation with all protein bound to the membrane with half the domain having 10 times more bound protein than the other. We then run the dynamics (M2) forward in time until we reach $\hat{t} = 38.4$, which is 4 minutes of real time, corresponding exactly to the time interval used in experiments. At $\hat{t} = 38.4$, we record the local density of PAR-3 on the anterior, which in dimensional variables is proportional to $A_a = F\hat{A}_a$. We then obtain the fraction of monomers on the anterior from (M5) and use this to compute α, which gives the mean oligomer size on the anterior as $1/(1-\alpha)^2$. We also record the A/P asymmetry at the end of the simulation. The results for our different feedback models are shown in Fig. M4. In the left panel, we show the mean oligomer size vs. the amount of bound PAR-3, which is based on polymerization kinetics and does not change when we change the feedback model.

In the right panel of Fig. M4, we show the A/P asymmetry as a function of mean oligomer

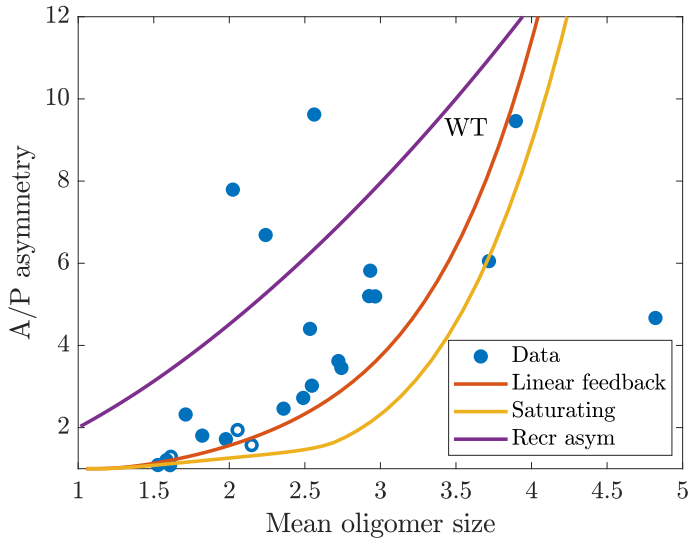

Figure M4: Dynamic PAR-3 depletion experiment.

size (on the anterior) for the different feedback models, compared to the experimental data. The red and yellow lines are when feedback saturates at a fixed *number* (model 1, red line) or fixed *percentage* (model 2, yellow line) of monomers. In this case, depleting the total amount of PAR-3 does not reduce (yellow lines) or even increases (red line) the relative amount of feedback for smaller amounts of PAR-3 (and smaller mean oligomer sizes). Because of this, the A/P asymmetries at these smaller mean oligomer sizes are *stable* for longer times, and so the model predicts the initial 10/1 asymmetry for smaller protein fractions will decrease to a smaller, but still stable, value.

By contrast, when the feedback saturates at a fixed fraction of the uniform state (model 3, purple line), depleting PAR-3 reduces the uniform state and reduces the feedback. Consequently, depleted embryos with smaller mean oligomer sizes *do not* exhibit bistable dynamics, and the asymmetries (of magnitude less than 5) that we see for mean oligomer sizes between 2 and 3 come from slow decay of the initial asymmetry to the uniform state. Seeing as this model matches the data best, we conclude that the asymmetries (of magnitude 2–5) for depleted PAR-3 amounts are consistent with asymmetries that are slowly dying out as the slow oligomerization dynamics equilibrate, while the larger asymmetries are consistent with bistability. That said, this feedback model predicts that increasing the amount of PAR-3 in the system will increase the relative amount of feedback, and gives asymmetries for large mean oligomer sizes that are much higher than wild type (a factor of 15 asymmetry when the mean anterior oligomer size is 4).

While our feedback models differ in the location of the pitchfork bifurcation that governs the

stability properties of the system, they all fundamentally predict a bifurcation from no asymmetry for mean oligomer sizes 2 or less to an asymmetry for larger mean oligomer sizes. We compare these predictions to a model based on recruitment asymmetry (in which case we simply set k_A^{on} to match the wild-type bound amount on the posterior and multiply the recruitment rate by 1.7 on the anterior), which predicts a persistent asymmetry even as the mean oligomer size drops to 1 (i.e., even without oligomerization). Thus, a recruitment asymmetry on the anterior half cannot explain the data, since it predicts that polarization can occur without oligomerization.

3.2 Phase diagram

We now use local perturbation analysis to prepare a phase diagram of the stability behavior for our "best" saturated feedback model (where the saturation scales so that the uniform state is stable). To do so, we set the parameters $\hat{K}_A^{\text{p}}$ and $\hat{K}_A^{\text{f}}$, determine the uniform steady state, and plot the attachment rate at constant cytoplasmic concentration (equal to that of the uniform state). We record the lowest and highest point where the two curves cross, then use these crossings to define an A/P ratio, with the higher point defining the mean oligomer size on the anterior. The resulting phase diagram is shown in Fig. M5, where we have added a black star to denote the wild type parameters.

3.3 Reducing feedback

4 Some text for conclusions

Unlike in budding yeast cells [10], there is no experimental evidence that *C. elegans* cells can spontaneously polarize, which means that the system is truly bistable. Traditionally, it has been speculated that the bistability comes from mutual inhibition of the aPAR and pPAR proteins [8, 13]. But translating this idea into equations becomes much harder than might be expected! Indeed, ODEs based on first-order mass action kinetics of aPAR-pPAR inhibition *do not* yield bistable dynamics under any choice of parameters [2]. Attempts to overcome this have used stoichiometric coefficients for the biochemical equations that guarantee bistability [6, 7] or included actomyosin flows designed to transport the aPARs only [12].

The experimental observations in this study provide a potential way out of this conundrum. It has long been known that disrupting PAR-3 [5] or its oligomerization [3] leads to a failure or severe disruption in establishing polarity. But our finding that PAR-3 asymmetries are stable

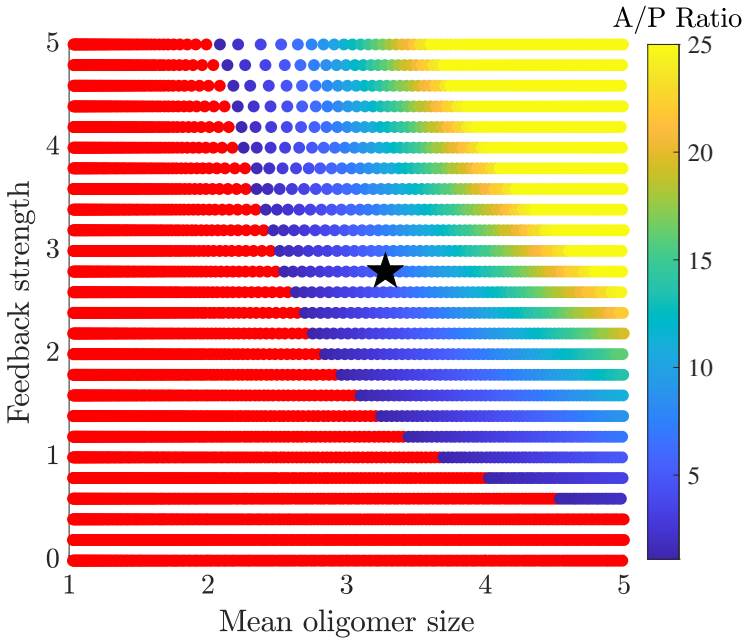

Figure M5: Phase diagram for PAR-3 asymmetries. We show steady states with various mean oligomer sizes on the anterior and differing feedback strengths $\hat{K}_A^{\mathrm{f}}$, where the saturation point scales so that the uniform steady state is stable for all choices of parameters. The red circles show the region of parameter space with a single stable state, while the blue–yellow circles show the region of bistability (color-coded based on the size of the A/P asymmetry). The black star denotes the parameters in the wild-type embryo.

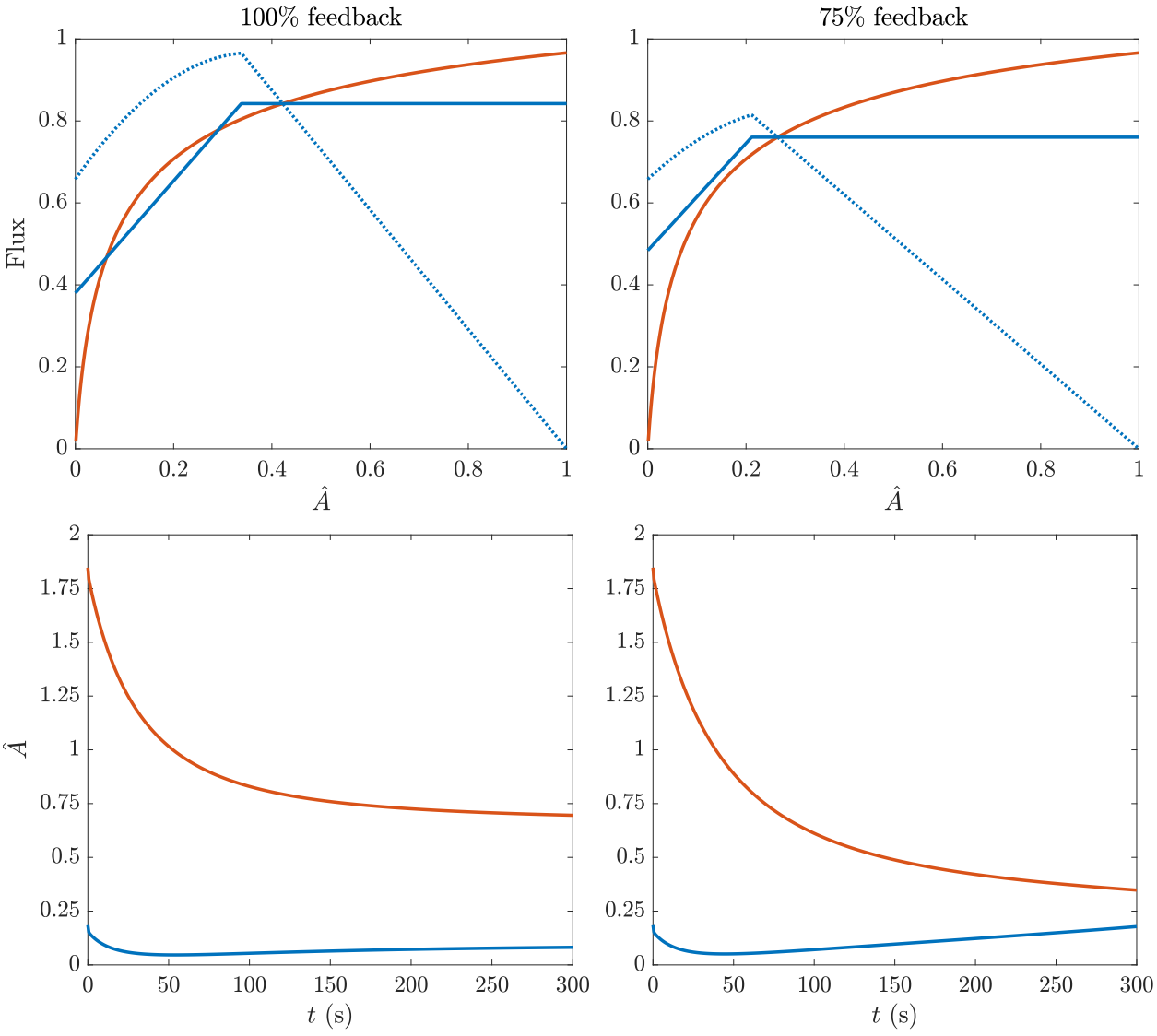

Figure M6: Reduced feedback for CDC-42.

even in the absence of posterior inhibitor PAR-1 [11] demonstrates that the dynamics of PAR-3 *by itself* are intrinsically bistable, and might therefore "anchor" the bistability of the entire PAR protein system. Our model therefore distinguishes itself from that of [9] by arguing for *bi*stability (described previously as "inducible polarization") rather than spontaneous *in*stability. The requirement for this bistability is that the "feedback" (recruitment of cytoplasmic monomers to the membrane by membrane-bound ones) must saturate at a point below the steady state, a regime which experimental observations strongly suggest the system operates in.

Given the intrinsic bistability of PAR-3, an exciting future direction is to introduce additional biochemistry and contractility into the model [11], and see if it can reproduce a stable boundary position under these circumstances. Because of the intrinsic bistability of PAR-3, we expect that first-order inhibition dynamics will be enough to generate bistability, which is in contrast to previous studies which did not account for the positive feedback of membrane-bound monomers promoting binding of cytoplasmic ones [2]. While this model is not meant to exclude other possible nonlinearities in the reaction kinetics [1], it does show that they are not strictly necessary for stable polarization.

References

[1] Tom Bland, Nisha Hirani, David Briggs, Riccardo Rossetto, KangBo Ng, Neil Q McDonald, David Zwicker, and Nathan W Goehring. Optimized dimerization of the par-2 ring domain drives cooperative and selective membrane recruitment for robust feedback-driven cell polarization. *bioRxiv*, pages 2023–08, 2023.

[2] Adriana T Dawes and Edwin M Munro. Par-3 oligomerization may provide an actin-independent mechanism to maintain distinct par protein domains in the early caenorhabditis elegans embryo. *Biophysical journal*, 101(6):1412–1422, 2011.

[3] Daniel J Dickinson, Francoise Schwager, Lionel Pintard, Monica Gotta, and Bob Goldstein. A single-cell biochemistry approach reveals par complex dynamics during cell polarization. *Developmental cell*, 42(4):416–434, 2017.

[4] Leah Edelstein-Keshet and G Bard Ermentrout. Models for the length distributions of actin filaments: I. simple polymerization and fragmentation. *Bulletin of mathematical biology*, 60(3):449–475, 1998.

[5] Bijan Etemad-Moghadam, Su Guo, and Kenneth J Kemphues. Asymmetrically distributed par-3 protein contributes to cell polarity and spindle alignment in early c. elegans embryos. *Cell*, 83(5):743–752, 1995.

[6] Nathan W Goehring, Philipp Khuc Trong, Justin S Bois, Debanjan Chowdhury, Ernesto M Nicola, Anthony A Hyman, and Stephan W Grill. Polarization of par proteins by advective triggering of a pattern-forming system. *Science*, 334(6059):1137–1141, 2011.

[7] Peter Gross, K Vijay Kumar, Nathan W Goehring, Justin S Bois, Carsten Hoege, Frank Jülicher, and Stephan W Grill. Guiding self-organized pattern formation in cell polarity establishment. *Nature physics*, 15(3):293–300, 2019.

[8] Jacob Halatek, Fridtjof Brauns, and Erwin Frey. Self-organization principles of intracellular pattern formation. *Philosophical Transactions of the Royal Society B: Biological Sciences*, 373(1747):20170107, 2018.

[9] Charles F Lang and Edwin M Munro. Oligomerization of peripheral membrane proteins provides tunable control of cell surface polarity. *Biophysical Journal*, 121(23):4543–4559, 2022.

[10] Alex Mogilner, Jun Allard, and Roy Wollman. Cell polarity: quantitative modeling as a tool in cell biology. *Science*, 336(6078):175–179, 2012.

[11] Anne Sailer, Alexander Anneken, Younan Li, Sam Lee, and Edwin Munro. Dynamic opposition of clustered proteins stabilizes cortical polarity in the c. elegans zygote. *Developmental cell*, 35(1):131–142, 2015.

[12] Filipe Tostevin and Martin Howard. Modeling the establishment of par protein polarity in the one-cell c. elegans embryo. *Biophysical journal*, 95(10):4512–4522, 2008.

[13] Philipp Khuc Trong, Ernesto M Nicola, Nathan W Goehring, K Vijay Kumar, and Stephan W Grill. Parameter-space topology of models for cell polarity. *New Journal of Physics*, 16(6):065009, 2014.